

Combining damage and fracture mechanics to model calving

J. Krug et al.

Combining damage and fracture mechanics to model calving

J. Krug^{1,2}, J. Weiss^{1,2}, O. Gagliardini^{1,2,3}, and G. Durand^{1,2}

¹CNRS, LGGE, 38041 Grenoble, France

²Univ. Grenoble Alpes, LGGE, 38041 Grenoble, France

³Institut Universitaire de France, Paris, France

Received: 3 February 2014 – Accepted: 6 February 2014 – Published: 14 February 2014

Correspondence to: J. Krug (jean.krug@ujf-grenoble.fr)

Published by Copernicus Publications on behalf of the European Geosciences Union.

This discussion paper is/has been under review for the journal The Cryosphere (TC).
Please refer to the corresponding final paper in TC if available.

Title Page

Abstract

Introduction

Conclusions

References

Tables

Figures

⏪

⏩

◀

▶

Back

Close

Full Screen / Esc

Printer-friendly Version

Interactive Discussion

brae, on the West coast of Greenland ice sheet the same year (Joughin et al., 2008a) are two examples of the impact of such perturbations on the behaviour of a glacier. In the sake of projecting ice sheet evolution, a deep understanding and representation of the processes occurring at the front are necessary, especially those concerning iceberg calving.

Among the several studies undertaken to model calving, the most used criterion is the one proposed by Nye (1957), according to whom the ability for a glacier to calve depends on the equilibrium between longitudinal stretching (opening term) and cryostatic pressure (closing term). This criterion has been used by several authors (e.g. Mottram and Benn, 2009; Nick et al., 2010; Otero et al., 2010; Nick et al., 2013) with successful results in representing the front variations of some major greenlandic and antarctic outlet glaciers. However, this model is based on a simple stress balance combined to an empirical criterion for calving. Consequently, it does not account for some physical aspects, such as the stress concentration at the tip of crevasses, or the crevasse depth, and so it may assess inaccurately the ice discharge in case of prognostic simulations.

Another approach to model calving has been done using particles models (Bassis and Jacobs, 2013; Åström et al., 2013). These models show interesting behaviours on describing the calving processes and the iceberg distribution, but are today inappropriate to describe large-scale ice-sheet flow due to their non-continuous approach.

For a few years, some authors have focused on continuum damage mechanics in order to represent both the development of micro-defects in the ice to the apparition of macro-scale crevasses, and their effects on the viscous behaviour of the ice while keeping a continuum approach. Initially applied to the deformation of metals (Kachanov, 1958), damage mechanics has been recently applied to ice dynamics to study the apparition of a single crevasse (Pralong et al., 2003; Pralong and Funk, 2005; Duddu and Waisman, 2013) or to average crevasse fields (Borstad et al., 2012). On the other hand, the elastic representation of fracturing processes using linear elastic fracture mechanics (van der Veen, 1998, 1997) has been employed to described the calving event itself, characterized by a rapid propagation of surface and bottom crevasses through the ice.

Combining damage and fracture mechanics to model calving

J. Krug et al.

Title Page

Abstract Introduction

Conclusions References

Tables Figures

⏪ ⏩

◀ ▶

Back Close

Full Screen / Esc

Printer-friendly Version

Interactive Discussion



Combining damage and fracture mechanics to model calving

J. Krug et al.

Title Page

Abstract

Introduction

Conclusions

References

Tables

Figures

◀

▶

◀

▶

Back

Close

Full Screen / Esc

Printer-friendly Version

Interactive Discussion

This approach has been rarely used in ice-sheet numerical modeling, however, as the representation of crevasses requires a high mesh refinement usually difficult to reach when modeling large glaciological bodies.

Here we consider a combined approach between damage mechanics and fracture mechanics. The proposed physically-based calving model can cover both the accumulation of damage as the ice is transported through the glacier, and the critical fracture propagation in the vicinity of the calving front. The slow development of damage represents the long timescales evolution of purely viscous ice, while the use of fracture mechanics allows to consider calving events occurring at short timescales, for which the ice can be considered as a purely elastic medium. The description of the physics implemented is presented in Sect. 2, covering the damage initiation and its development, the fracture propagation and its arrest criterion. In Sect. 3, sensitivity tests are carried on Helheim Glacier, and results are discussed.

2 Physics of the model

2.1 Governing equations for ice flow

2.1.1 Ice flow and rheology

We consider an incompressible, isothermal and gravity-driven ice-flow in which the ice exhibits a non-linear viscosity. The ice flow is ruled by the Stokes equations (i.e. Navier–Stokes equations without any inertial term), meaning the momentum and the mass balance:

$$\operatorname{div}(\boldsymbol{\sigma}) + \rho_i \mathbf{g} = 0 \quad (1)$$

$$\operatorname{div}(\mathbf{u}) = 0 \quad (2)$$

where $\boldsymbol{\sigma}$ represents the Cauchy stress tensor, \mathbf{g} the gravity force vector, ρ_i the density of ice and \mathbf{u} the velocity vector. The Cauchy stress tensor can be expressed as a func-

tion of the deviatoric stress tensor \mathbf{S} and the isotropic pressure p with $\boldsymbol{\sigma} = \mathbf{S} - p\mathbf{I}$ and $p = -\text{tr}(\boldsymbol{\sigma})/3$. Ice rheology is represented by a non-linear Norton–Hoff type flow law called *Glen’s flow law*, which reads:

$$\mathbf{S} = 2\eta\dot{\boldsymbol{\epsilon}} \quad (3)$$

This equation links the deviatoric stress tensor \mathbf{S} to the strain rate tensor $\dot{\boldsymbol{\epsilon}}$. The effective viscosity η writes:

$$\eta = \frac{1}{2}(EA)^{-1/n} \mathbf{I}_{\dot{\boldsymbol{\epsilon}}_2}^{(1-n)/n} \quad (4)$$

where $\mathbf{I}_{\dot{\boldsymbol{\epsilon}}_2}^2$ represents the square of the second invariant of the strain rate tensor, A is the fluidity parameter and E is an *enhancement factor*, usually varying between 0.58 and 5.6 for ice-flow models (Ma et al., 2010).

2.1.2 Boundary conditions

The upper surface is defined as a stress-free surface, and therefore obeys the following equation:

$$\frac{\partial z_s}{\partial t} + u_s \frac{\partial z_s}{\partial x} + v_s \frac{\partial z_s}{\partial y} - w_s = a_s \quad (5)$$

where z_s refers to the elevation of the top surface, and (u_s, v_s, w_s) are the surface velocities. The surface mass balance a_s is prescribed as a vertical component only. As we neglect any effect of atmospheric pressure, normal and tangential stresses at the surface are zero:

$$\sigma_{nn}|_s = 0$$

$$\sigma_{nt_i}|_s = 0 \quad (i = 1, 2)$$

Subscripts n and t_i respectively refers to normal (pointing outward) and tangential directions.

Similar to the upper free surface, the bottom surface is described by:

$$\frac{\partial z_b}{\partial t} + u_b \frac{\partial z_b}{\partial x} + v_b \frac{\partial z_b}{\partial y} - w_b = a_b \quad (6)$$

where (u_b, v_b, w_b) are the basal velocities, and a_b represents the vertical component of the basal mass balance (melting or accretion). At the bed, the glacier can be either grounded or floating. The grounded part of the glacier undergoes a shearing stress which is represented by a non-linear Weertman-type friction law reading:

$$\mathbf{u} \cdot \mathbf{n} = 0$$

$$\sigma_{nt_i}|_b = t_i \cdot (\boldsymbol{\sigma} \cdot \mathbf{n})|_b = C u_b^{m-1} u_{t_i} \quad (i = 1, 2)$$

where C and $m = 1/3$ are the friction coefficient and the friction exponent respectively. u_b is the norm of the sliding velocity $\mathbf{u}_b = \mathbf{u} - (\mathbf{u} \cdot \mathbf{n}_b) \mathbf{n}_b$, with \mathbf{n}_b the normal outward-pointing unit vector to the bedrock. Where the ice is floating the free surface is forced by an external sea pressure normal to the surface:

$$\sigma_{nn}|_b = -\rho_w g (l_w - z_b)$$

$$\sigma_{nt_i}|_b = 0 \quad (i = 1, 2)$$

where ρ_w is the water density, l_w the sea level, and z_b refers to the elevation of bottom surface. The position between the grounded and floating part of the basal boundary, i.e. the grounding line, is part of the solution and computed solving a contact problem following Durand et al. (2009) and Favier et al. (2012). The basal friction C is determined using the inverse method described in Jay-Allemand et al. (2011). This method consists in inferring the basal friction parameter by reducing the mismatch between observed and modeled surface velocities.

Combining damage and fracture mechanics to model calving

J. Krug et al.

Title Page

Abstract

Introduction

Conclusions

References

Tables

Figures

⏪

⏩

◀

▶

Back

Close

Full Screen / Esc

Printer-friendly Version

Interactive Discussion



The front is defined as a third free-surface, which can undergo melting, and follows the equation:

$$\frac{\partial x_f}{\partial t} + v_f \frac{\partial x_f}{\partial y} + w_f \frac{\partial x_f}{\partial z} - u_f = a_f \quad (7)$$

5 where (u_f, v_f, w_f) are the frontal velocities, and a_f characterizes the frontal mass balance. The front undergoes water back pressure where the ice stands under sea level and a stress-free condition above sea level. These Neumann conditions read:

$$\sigma_{nn}|_f = -\max(\rho_w g(l_w - z), 0)$$

$$10 \sigma_{nt_i}|_f = 0 \quad (i = 1, 2)$$

The list of physical and numerical parameters used in this paper is given in Table 1. Some boundary conditions are specific to the 2-D flowline application conducted in Sect. 3. More details about these specific boundaries are given in Sect. 3.2.

2.2 Continuum damage mechanics model

15 Continuum Damage Mechanics (CDM) was first proposed by Kachanov (1958) to quantify the degradation of mechanical properties resulting from the nucleation of internal defects such as microcracks or voids. As stated by Lemaitre et al. (1988), CDM describes the evolution of phenomena in the medium from a virgin state to the initiation of macroscopic fracture. The major interest of this approach is that the material is still
 20 considered as a continuous material, even when the level of damage is high. The slow deformation is typically encountered in glaciological media, where the ice flows slowly under its own weight along the slope of the surface. CDM has been successfully used in ice-flow models to deal with some glaciological issues such as the flow acceleration of large damaged areas or the opening of crevasses in hanging glaciers (Xiao and Jordaan, 1996; Pralong et al., 2003; Pralong and Funk, 2005; Jouvet et al., 2011; Borstad
 25 et al., 2012).

Title Page	
Abstract	Introduction
Conclusions	References
Tables	Figures
⏪	⏩
◀	▶
Back	Close
Full Screen / Esc	
Printer-friendly Version	
Interactive Discussion	



Combining damage and fracture mechanics to model calving

J. Krug et al.

Title Page

Abstract

Introduction

Conclusions

References

Tables

Figures

◀

▶

◀

▶

Back

Close

Full Screen / Esc

Printer-friendly Version

Interactive Discussion

The principle of CDM models is based on the use of a damage variable, usually denoted D , which represents the degradation of mechanical properties (stiffness, viscosity, ...) resulting from a population of defects whose effect is averaged at a mesoscale. When considering an anisotropic approach, damage must be represented as a second order tensor (Murakami and Ohno, 1981; Pralong and Funk, 2005). As stated by Rist et al. (1999), considering damage as isotropic is sufficient when dealing with glaciological bodies such as glaciers or ice-sheets. In this case, as it is assumed here, the state variable D is a scalar quantity. For non-damaged ice $D = 0$, and $0 < D < 1$ when ice is damaged. A fully damaged ice is obtained when $D \rightarrow 1$.

To describe the stress altered by the amount of damage, an effective stress is introduced:

$$\tilde{\sigma} = \frac{\sigma}{(1-D)}, \quad (8)$$

with $\tilde{\sigma}$ the effective Cauchy stress tensor. This effective stress can be understood as the original force applied on an effective undamaged area only. Using the equivalence principle of Lemaitre et al. (1988), strain is affected by the damage only through the effect of an effective stress entering the rheological law (see Eq. 3) at the place of σ . Thereby, there is no need to define an effective strain rate.

2.2.1 Damage evolution

Damage is a property of the material at the mesoscale. It is therefore advected by the ice flow, and evolves through time depending on the stress field. To take this evolution into account, we prescribe an advection equation reading:

$$\frac{\partial D}{\partial t} + \mathbf{u} \nabla D = \begin{cases} f(\chi) & \text{if } f(\chi) > 0 \\ 0 & \text{otherwise} \end{cases} \quad (9)$$

where the right hand side represents a damage source term $f(\chi)$. This term can be written as a function of a damage criterion χ and a numerical parameter B , thereafter

for sub-grid scale heterogeneity, we introduce some noise on the value of σ_{th} : $\sigma_{th} = \overline{\sigma_{th}} \cdot (1 + \sigma_{var})$, where σ_{var} follows a gaussian distribution with a standard deviation of 0.05. $\overline{\sigma_{th}}$ usually reaches several tens of kilo-Pascals (Pralong and Funk, 2005). Sensitivity of the model to this parameter will be discussed in Sect. 3.

This formulation of the damage criterion implies some assumptions on the behaviour of ice. In particular, the ice cannot be damaged under compression or pure shear. However, it remains consistent with the approach of Benn et al. (2007), according to which the longitudinal stretching associated to longitudinal velocity gradients can be seen as a first order process controlling the development of crevasses in glaciers. Moreover, it is consistent with the fracture mechanics approach explained in Sect. 2.3 which considers crevasses opening in pure tension only.

2.2.2 Viscosity modification

As pointed by Pralong et al. (2003) and Pralong and Funk (2005) on alpine hanging glaciers, the ice flow is altered by the accumulation of micro-defects in the ice: damage softens the ice and accelerates the creep. This softening is taken into account through the introduction of the effective stress within Glen's law.

When introducing the effective deviatoric stress tensor $\tilde{\mathbf{S}}$ and taking into account the equivalence principle, as described in Sect. 2.2, Eq. (3) reads:

$$\tilde{\mathbf{S}} = (A)^{-1/n} \mathbf{I}_{\dot{\boldsymbol{\varepsilon}}_2}^{(1-n)/n} \dot{\boldsymbol{\varepsilon}} \quad (12)$$

When combined with Eq. (8), it comes:

$$\mathbf{S} = (A)^{-1/n} (1 - D) \mathbf{I}_{\dot{\boldsymbol{\varepsilon}}_2}^{(1-n)/n} \dot{\boldsymbol{\varepsilon}} \quad (13)$$

By identification with Eq. (3), one can link the enhancement factor E with the damage D , such as

$$E = \frac{1}{(1 - D)^n} \quad (14)$$

Combining damage and fracture mechanics to model calving

J. Krug et al.

Title Page

Abstract

Introduction

Conclusions

References

Tables

Figures

⏪

⏩

◀

▶

Back

Close

Full Screen / Esc

Printer-friendly Version

Interactive Discussion



It comes that for undamaged ice (meaning $D = 0$), $E = 1$, and so the flow regime is unchanged. When the damage increases ($D > 0$), $E > 1$, the viscosity of the ice is reduced, and so the velocity of the flow increases. This formulation of the enhancement factor is consistent with the expected behaviour, and it has already been used in previous studies, such as Borstad et al. (2012). The damage then evolves under the effect of the stress field, where the ice undergoes pure tension, and it exerts a positive feedback on the velocity field.

2.3 Fracture mechanics

Continuum damage mechanics is a reliable tool to deal with the degradation of ice viscosity with increasing damage over long timescales. It can be understood as a way to simulate sub-critical crevasse nucleation and propagation (Weiss, 2004) at a meso-scale, and its role on creep enhancement. However, calving events are triggered by rapid propagation of preexisting fractures, at very short timescales and speeds reaching a significant fraction of the speed of sound. Thus, this process cannot be represented by a viscous rheology (Weiss, 2004). Instead, at such short timescales, the medium should be considered as elastic. In these conditions, Linear Elastic Fracture Mechanics (LEFM) provides a useful tool to account for these features and matches pretty well with the observations done on crevasse depths (Mottram and Benn, 2009). The application of LEFM on penetration of surface crevasses, originally introduced by Smith (1976), was used by several authors since then (Rist et al., 1999; van der Veen, 1998, 1997; Nath and Vaughan, 2003). Here, a LEFM model is combined to the damage model previously described to achieve the formulation of a calving law taking into account several processes occurring in the glacier. In LEFM, three modes of crack propagation can be considered: Mode I, Mode II and Mode III, which respectively refer to simple opening, sliding and tearing. In the following, only the opening mode (Mode I) is considered.

Combining damage and fracture mechanics to model calving

J. Krug et al.

Title Page

Abstract

Introduction

Conclusions

References

Tables

Figures

⏪

⏩

◀

▶

Back

Close

Full Screen / Esc

Printer-friendly Version

Interactive Discussion



2.3.1 LEFM theory

The key physical parameter of LEFM is the stress intensity factor K . van der Veen (1998) gives a formula for K_I in an idealized case where the opening stress is constant in the vertical direction. For opening mode, we can define a coordinate system in the space of principal stresses (x', y', z) , in which K_I reads:

$$K_I = \beta S_{x'x'} \sqrt{\pi d} \quad (15)$$

where $S_{x'x'}$ is the principal component of the deviatoric stress tensor (independent of depth), d is the crevasse depth and β is a parameter depending on the geometry of the problem. We consider that the crack propagation occurs in the plane which is perpendicular to the first principal direction. In the ideal case introduced by van der Veen (1998), fracture propagation was a function of the difference between the opening full stress $\sigma_{x'x'}$ resulting from horizontal velocity gradients, and the cryostatic pressure (*creep closure*) $\sigma_p = \rho_i g z$ corresponding to the weight of the ice.

However, when considering real cases, the opening term $\sigma_{x'x'}$ (and so $S_{x'x'}$) is not constant over depth z or lateral coordinate y' . Consequently, the appropriate formula to calculate the stress intensity factor for an arbitrary stress profile $S_{x'x'}(y', z)$ applied to the crack is given by the weight functions method (Labbens et al., 1974):

$$K_I = \int_{y'=y_1}^{y'=y_r} \int_{z=0}^{z=d} \beta(z, d, H) S_{x'x'}(y', z) dy dz \quad (16)$$

where $y_1 - y_r$ refers to the glacier width (see Fig. 2). This formula lays on the use of the superposition principle: in the case of linear elasticity, the value of the stress intensity factor at the tip of the crack can be seen as the sum of all individuals point loads along the crack length. In our case, instead of considering the value of the along-flow component of the deviatoric stress tensor at the tip of the crack, we multiplied it by

Combining damage and fracture mechanics to model calving

J. Krug et al.

Title Page

Abstract

Introduction

Conclusions

References

Tables

Figures

⏪

⏩

◀

▶

Back

Close

Full Screen / Esc

Printer-friendly Version

Interactive Discussion

of water in crevasses adds a supplementary force $\rho_w g d_w$, where d_w is the water depth. This supplementary hydrostatic pressure, added to the tensile opening stress, counteracts the cryostatic pressure. It has been shown that water-filled crevasses are able to propagate the full thickness of the glacier as soon as the level of water in the crevasse exceeds several meters. Without this feature, our model is sufficient to provide a lower bound for crevasse propagation. It is worth noting, however, that the introduction of such a mechanism in our framework would be straightforward, once the water level within crevasses can be defined independently.

2.3.3 Fracture arrest

Once the conditions for fracture initiation are fulfilled, we consider that the crevasse propagates vertically. In van der Veen (1997), crevasses propagate downward as long as the inequation $K_I \geq K_{Ic}$ is satisfied, thus assuming that $K_I = K_{Ic}$ represents both a crack propagation and a crack arrest criterion. Such arrest criterion is probably misleading, as the stress intensity factor at arrest, though non-zero, is always lower than the stress intensity factor at propagation (Ravi-Chandar and Knauss, 1984), mostly as dynamical effects have to be taken into account for the arrest condition. Therefore, following Ravi-Chandar, we use a crevasse arrest criterion: $K_I < K_{Ia}$, with $K_{Ia} = \alpha K_{Ic}$ and $0 < \alpha < 1$. The value of α for ice is unknown. In the following, we arbitrarily set α to 0.5. Sensitivity to this value will be discussed in Sect. 3.3.4.

The computation of the stress intensity factor using the weight function described in Eq. (16), leads to a singularity as $d/H \rightarrow 1$. Consequently, the arrest criterion is computed at a depth d_f equals to 90 % of the ice thickness. We assumed that a crevasse which propagated through 90 % of the glacier thickness propagates the full thickness. Thereby, the stress intensity factor is computed at d_f and if $K_{I|d_f} \geq K_{Ia}$, the calving occurs.

This framework has two consequences. Firstly, the stress profile $S_{x',x'}$ used to calculate $K_{I|d_f}$ for the arrest criterion is estimated before the propagation of the crevasse. This propagation modifies $S_{x',x'}$, but this effect is not considered here. Secondly, if the

which the last 15 km of the glacier are well represented. In this dataset, the initial front position corresponds to the May 2001 pre-collapse geometry. In addition, we choose to consider the glacier as isothermal over its terminating part, by prescribing a constant temperature of -4.6°C , following Nick et al. (2009) again. The constant surface mass balance a_s is taken from Cook (2012) who fitted direct observations from stakes placed over the glacier between 2007 and 2008, which are assumed to represent the annual surface mass balance.

3.2 Flowline specificities and numerics

Following our notation system, the ice flows along the horizontal Ox direction and perpendicular to a vertical Oz axis. As we are working in two dimensions, the coordinate system (x', y', z) defined in Sect. 2.3.1 and the coordinate system (x, y, z) are identical.

The geometry covers the last 30 km of the glacier, with an average thickness varying between 900 m at the inlet boundary, and 700 m at the front. Using the metric from Nick et al. (2009), the beginning of the mesh is located at kilometer 319, and the front at kilometer 347 (see Fig. 5). This geometry is discretized through a structured mesh of 4900 quadrilateral elements, refined on the upper surface and at the front. The size of the elements varies from 300 m to 50 m at the front in the horizontal direction, and from 50 m to 5 m on the upper surface in the vertical direction. Sensitivity tests have been carried out to optimize mesh size: by enhancing the number of element to 15 000, the general behaviour of the model remains unchanged (not shown). The most important criterion to be considered is the element size in the vicinity of the upper surface to allow both damage development and fracture initiation. The final refinement fulfill the need for a proper damage advection (and thus avoiding mesh dependency) and an efficient serial computation. We employed an Arbitrary Lagrangian Eulerian (ALE) method to take into account ice advection and mesh deformation.

The specific boundary conditions adopted for the 2-D application are precised below, otherwise the boundary conditions are those presented in Sect. 2.1.2.

TCO

8, 1111–1150, 2014

Combining damage and fracture mechanics to model calving

J. Krug et al.

Title Page

Abstract

Introduction

Conclusions

References

Tables

Figures

⏪

⏩

◀

▶

Back

Close

Full Screen / Esc

Printer-friendly Version

Interactive Discussion

The basal friction C is inferred from the surface velocity data for year 2001 presented in Howat et al. (2007).

In order to represent melting at the calving front, we prescribe an ablation function, linearly increasing with depth, with a zero value at sea level. This constant melting parametrization of 1 m day^{-1} is inspired from the work of Rignot et al. (2010) on four West Greenland glaciers.

The inflow boundary condition ($x = 319 \text{ km}$) does not correspond to an ice divide. As we consider only the last kilometers before terminus, we made the assumption that the velocity of ice is constant over depth at the upstream boundary, and we impose a Dirichlet condition corresponding to a constant horizontal velocity $u_x = 4000 \text{ m a}^{-1}$, in agreement with the observed surface velocity from Howat et al. (2007).

When dealing with a 2-D flowline representation of the flow, we have to take into account some three-dimensional aspects. Especially, lateral friction along the rocky-margins of the glacier can play a significant role, by adding a resistive stress to the flow. Here, it is prescribed through a modified gravity force using a lateral friction coefficient k , as proposed by Gagliardini et al. (2010). This coefficient, which reads:

$$k = \frac{(n+1)^{1/n}}{W^{\frac{n+1}{n}} (2A)^{1/n}} \quad (17)$$

highly depends on the Glen's flow law parameters A and n , as well as on the channel width W (taken from Nick et al., 2009).

Even if the velocity and the surface topography are known and correspond to the observed state of the glacier in May 2001, some adjustments must be made in order to obtain a stable steady state, before running sensitivity tests (Gillet-Chaulet et al., 2012). We let the geometry adjust to the prescribed boundary conditions and inversed basal friction for approximately 8 yr.

Combining damage and fracture mechanics to model calving

J. Krug et al.

Title Page

Abstract

Introduction

Conclusions

References

Tables

Figures

⏪

⏩

◀

▶

Back

Close

Full Screen / Esc

Printer-friendly Version

Interactive Discussion



3.3 Results and discussion

3.3.1 Calibration of the model: sampling strategy

As mentioned in the previous sections, the acceptable ranges for three parameters σ_{th} , B , and D_c have to be evaluated. This is obtained thanks to a latin hypercube sampling. This methods requires a number of variables to be tested, and a number of simulations. As the exact values for our parameters are unknown, these are randomly sampled between given ranges. The stress threshold σ_{th} is estimated to be within the range of [0.02,0.2] MPa. The lower bound is near to the one given in Pralong and Funk (2005). If $\sigma_{th} > 0.2$, the stress field is not high enough to reach the damage threshold, and damaging never happens. The Damage enhancement factor B is related to the rate at which the damage increases, once the damage criterion χ is positive. This value is particularly difficult to evaluate, especially because it does not lay on laboratory experiments or observations. Thus, we choose a large range [0.5,3]. However, one must note that this parameter should have a value which keeps the stress field in the vicinity of the damage envelope, once the stress has been released by damaging. The critical damage value D_c has already been documented (Pralong and Funk, 2005; Borstad et al., 2012; Duddu and Waisman, 2013). According to their values, we set our range within [0.4,0.6]. The number of computed simulations was 250.

3.3.2 Calibration of the model: spin-up

Damage can be produced anywhere in the glacier. As we need to obtain a steady state for the damage field, it is necessary to let the damage created upstream be advected to the front. This spin-up lasts 8 yr. During this period, the front is maintained at its initial position, without submarine frontal melting, and the procedure of calving is not activated. Once the steady state is obtained, the front is released, the frontal melting is prescribed and the calving procedure is activated.

Title Page

Abstract

Introduction

Conclusions

References

Tables

Figures



Back

Close

Full Screen / Esc

Printer-friendly Version

Interactive Discussion

3.3.3 Model response

As mentioned in Andresen et al. (2011), over the last century, Helheim Glacier has probably undergone several advance and retreat cycles, and observations of sand deposits imply a variation of the terminus around less than 10 km. The knowledge about the potential triggering mechanisms for retreat cycles is still poor: according to Joughin et al. (2008b) and Andresen et al. (2011), this retreat may have been forced by an enhanced summer temperature, and higher ocean water temperature, although sensitivity of calving to temperature remains unclear.

For these reasons, we did not try to reproduce the precise chronology of the Helheim's recent retreat in this paper. Instead, we study the dynamical behaviour of the model with respect to the different sets of parameters, and try to distinguish between unrealistic and realistic behaviours. The simulations presented in the previous sections were run during 4 yr after the spin-up. Among the 250 sets of parameters, the model response can be split in 3 classes, illustrated in Fig. 6. The blue curve on this figure represents a case where the calving almost never happened, and where the glacier advances too much, creating a floating tongue of several tens of kilometers. The yellow curve illustrates a case where the calving occurs too quickly, leading to a front retreat far upstream. The red curve represents a case consistent against observations, where the front of the glacier is punctuated by irregular calving events, forcing the glacier to keep its extent in an acceptable range of values.

This classification in three classes of behaviour can be generalized to the 250 simulations. In order to eliminate aberrant behaviour, we prescribe a sanity-check, by considering plausible sets of parameters as the ones which lead to a simulated front position within the range $[340 \text{ km}, 350 \text{ km}]$. The results are represented in Fig. 7, in the space of parameter $(B, \bar{\sigma}_{\text{th}})$. On this figure, we distinguished once again the same three classes, blue plus signs, yellow crosses and red diamonds, representing respectively the case where the front exceeds 350 km, the case where the front retreats more inland than

Combining damage and fracture mechanics to model calving

J. Krug et al.

Title Page

Abstract

Introduction

Conclusions

References

Tables

Figures



Back

Close

Full Screen / Esc

Printer-friendly Version

Interactive Discussion

Combining damage and fracture mechanics to model calving

J. Krug et al.

Title Page

Abstract

Introduction

Conclusions

References

Tables

Figures

⏪

⏩

◀

▶

Back

Close

Full Screen / Esc

Printer-friendly Version

Interactive Discussion

resented on Fig. 8a and b, damage increases in the area where the traction is high enough to exceed $\overline{\sigma_{th}}$, meaning over the bumps. This is consistent with observations of glaciers flowing over slope ruptures (Pralong and Funk, 2005). Here, the value of $\overline{\sigma_{th}}$ is low enough, and the damage develops over a depth of almost 15 m, at a rate high enough to reach the critical damage value D_c at the front and initiate calving.

Mottram and Benn (2009) investigated crevasse depth in the vicinity of the terminus of a Svalbard tidewater calving glacier, and showed that most of crevasses were under 10 m depth. In our experiments, damage develops at depths around 5 m to 15 m when calving usually occurs. As described previously, this value of d must be high enough to account for critical crevasse propagation, and is consistent with observations.

The parameter D_c is a control on whether the fracture propagates or not. If it is low, the conditions for crevasse propagation may occur easily, as soon as the criterion on LEFM is fulfilled. On the contrary, if D_c is too high, damage may never reach a sufficient depth to initiate fracture propagation. As a consequence, the value of D_c controls the location of the calving front. However, D_c is tightly linked with $(B, \overline{\sigma_{th}})$ through the production of damage upstream and it must be chosen in the same range as the level of damage at the front.

After the sensitivity to the three main numerical parameters $\overline{\sigma_{th}}$, B , and D_c has been realized, the influence of other parameters discussed above has been undertaken. Results showed that the model response is not sensitive to the parameters K_{lc} and α (not shown). As described in Eq. (16), the stress intensity factor strongly increases with crevasse depth. As the cryostatic pressure does not strongly increase with depth near the calving front, the value of S_{xx} remains high enough. As a consequence, K_I increases with depth. In addition, as $K_{la} \leq K_{lc}$ whatever α , once the crevasse propagation is initiated, it does not end before reaching the bedrock, at least for the configuration modeled here.

At last, the sensitivity to the initial heterogeneous micro-defects distribution introduced in Sect. 2.2.1 has been tested. The standard deviation of the distribution of stress threshold $\overline{\sigma_{th}}$ was varied within the range [0.005, 0.2]. Results show that the

Combining damage and fracture mechanics to model calving

J. Krug et al.

Title Page

Abstract

Introduction

Conclusions

References

Tables

Figures

⏪

⏩

◀

▶

Back

Close

Full Screen / Esc

Printer-friendly Version

Interactive Discussion

consistency of the behavior remains unchanged, but the spatial and temporal variability of the front position is modified (not shown). A higher standard deviation leads to a higher variability in the front position. In addition, we investigated the natural variability of the model. Repeating the same simulation several times does not change the general behaviour of the model. However, it modifies both the temporal and spatial frequency of calving events (not shown). These results highlight the existence of an intrinsic variability of the glacier.

According to our sanity check, among the 250 simulations, 36 presents a realistic behaviour. These experiments totalize about 1000 calving events. The distribution of front retreats is given in Fig. 9. Most of the events correspond to a retreat of the front between 300 m to 1000 m upstream, despite some larger events. This figure should not be interpreted as icebergs size distribution. Indeed, one must distinguish between the front retreat and the size of resulting iceberg(s), which may be strongly different, as the calved portion of ice can fragment into many icebergs and/or capsizes. However, distribution of the distance of front retreat may remain an interesting parameter to validate the model, but it would require a continuous tracking of the front position of the actual glacier, as discrete determination of the position (Joughin et al., 2008b) may bias the estimation of the retreat of single events. We are not aware of the existence of such a dataset existing on Helheim glacier.

Obviously, in the experiments presented in this paper, the cycles of advance and retreat which can be observed on Fig. 6 are not related to any variability in the external forcing, but depends on the own dynamics of the glacier. This brings us to the conclusion that a variation of the front position of several kilometers may be related to the glacier internal dynamics and are not necessarily the consequence of an external forcing.

4 Conclusions

In this work, we combined continuum damage mechanics and linear elastic fracture mechanics to propose a physically-based calving model able (i) to reproduce the slow development of small fractures leading to the apparition of macroscopic crevasse fields, over long timescales, while considering ice as a viscous material, and (ii) to deal with the elastic behaviour of breaking ice, consistent with the critical crevasse propagation triggering calving events, characterized by very short timescales. The model has been applied to Helheim Glacier, which allowed to constrain the acceptable sets of parameters. In this case, the front was dynamically maintained within the same extent as the one observed during the last century.

We showed that the ability of the model to have a realistic behaviour lays on a balance between the three damage parameters ($\bar{\sigma}_{th}$, B , and D_c). The first two parameters must be in a range which allows the damage to develop sufficiently in the damaging areas before being transported downstream. Then, the maximal value of damage reaching the front should be close to D_c and at a sufficient depth in order to trigger calving.

One must keep in mind that this sensitivity test is based on the response of one specific glacier to a poorly known external forcing and with limited observations. In these conditions, we show that some sets of parameters definitely generate a reliable behaviour, but one should be careful when considering another configuration, and make sure that the response of the model is realistic. Despite this limitation, this calving model based on realistic physical approaches gives reliable results and could be easily implemented in classical ice-flow finite element models.

The calving process described in this paper is immediately driven by the variation in longitudinal stretching associated with horizontal velocity gradients, producing a first-order control on calving rate, as stated by Benn et al. (2007). Local aspects, involving undercutting or force imbalance at ice cliffs are described as second-order calving pro-

Combining damage and fracture mechanics to model calving

J. Krug et al.

Title Page

Abstract

Introduction

Conclusions

References

Tables

Figures

⏪

⏩

◀

▶

Back

Close

Full Screen / Esc

Printer-friendly Version

Interactive Discussion

cesses. Using this model, further work could be undertaken in enhancing the general knowledge of these second-order phenomena.

Appendix A

Weight function for stress intensity factor

- 5 As stated by Glinka (1996), the weight function for the computation of the stress intensity factor depends on the specific geometry of the initial crack. For an edge crack in a finite width plate, the weight function is given by:

$$\beta(y, d) = \frac{2}{\sqrt{2\pi(d-y)}} \left[1 + M_1 \left(1 - \frac{y}{d}\right)^{1/2} + M_2 \left(1 - \frac{y}{d}\right)^1 + M_3 \left(1 - \frac{y}{d}\right)^{3/2} \right]$$

- 10 The weight function depends on 3 numerical parameters, polynomial functions of the ratio d/H . They read:

$$\begin{aligned} M_1 = & 0.0719768 - 1.513476 \left(\frac{d}{H}\right) - 61.1001 \left(\frac{d}{H}\right)^2 + 1554.95 \left(\frac{d}{H}\right)^3 \\ & - 14583.8 \left(\frac{d}{H}\right)^4 + 71590.7 \left(\frac{d}{H}\right)^5 - 205384 \left(\frac{d}{H}\right)^6 + 356469 \left(\frac{d}{H}\right)^7 \\ & - 368270 \left(\frac{d}{H}\right)^8 + 208233 \left(\frac{d}{H}\right)^9 - 49544 \left(\frac{d}{H}\right)^{10} \end{aligned}$$

$$\begin{aligned} M_2 = & 0.246984 + 6.47583 \left(\frac{d}{H}\right) + 176.456 \left(\frac{d}{H}\right)^2 - 4058.76 \left(\frac{d}{H}\right)^3 \\ 15 & + 37303.8 \left(\frac{d}{H}\right)^4 - 181755 \left(\frac{d}{H}\right)^5 + 520551 \left(\frac{d}{H}\right)^6 - 904370 \left(\frac{d}{H}\right)^7 \end{aligned}$$

Combining damage and fracture mechanics to model calving

J. Krug et al.

Title Page

Abstract

Introduction

Conclusions

References

Tables

Figures

◀

▶

◀

▶

Back

Close

Full Screen / Esc

Printer-friendly Version

Interactive Discussion



Bevan, S. L., Luckman, A. J., and Murray, T.: Glacier dynamics over the last quarter of a century at Helheim, Kangerdlugssuaq and 14 other major Greenland outlet glaciers, *The Cryosphere*, 6, 923–937, doi:10.5194/tc-6-923-2012, 2012. 1125

Borstad, C. P., Khazendar, A., Larour, E., Morlighem, M., Rignot, E., Schodlok, M. P., and Seroussi, H.: A damage mechanics assessment of the Larsen B ice shelf prior to collapse: toward a physically-based calving law, *Geophys. Res. Lett.*, 39, L18502, doi:10.1029/2012GL053317, 2012. 1113, 1117, 1121, 1128

Cook, S. J.: Environmental Controls on Calving in Grounded Tidewater Glaciers, Ph.D. thesis, Swansea University, 2012. 1125, 1126

Depoorter, M., Bamber, J., Griggs, J., Lenaerts, J., Ligtenberg, S., van den Broeke, M., and Moholdt, G.: Calving fluxes and basal melt rates of Antarctic ice shelves, *Nature*, advance online publication, 1, 2013. 1112

Duddu, R. and Waisman, H.: A temperature dependent creep damage model for polycrystalline ice, *Mech. Mater.*, 46, 23–41, 2012. 1119

Duddu, R. and Waisman, H.: A nonlocal continuum damage mechanics approach to simulation of creep fracture in ice sheets, *Comput. Mech.*, 51, 1–14, 2013. 1113, 1119, 1128

Durand, G., Gagliardini, O., De Fleurian, B., Zwinger, T., and Le Meur, E.: Marine ice sheet dynamics: hysteresis and neutral equilibrium, *J. Geophys. Res.-Earth*, 114, F03009, doi:10.1029/2008JF001170, 2009. 1116

Favier, L., Gagliardini, O., Durand, G., and Zwinger, T.: A three-dimensional full Stokes model of the grounding line dynamics: effect of a pinning point beneath the ice shelf, *The Cryosphere*, 6, 101–112, doi:10.5194/tc-6-101-2012, 2012. 1116

Fischer, M., Alley, R., and Engelder, T.: Fracture toughness of ice and firn determined from the modified ring test, *J. Glaciol.*, 41, 383–394, 1995. 1123

Gagliardini, O., Durand, G., Zwinger, T., Hindmarsh, R., and Le Meur, E.: Coupling of ice-shelf melting and buttressing is a key process in ice-sheets dynamics, *Geophys. Res. Lett.*, 37, L14501, doi:10.1029/2010GL043334, 2010. 1112, 1127

Gagliardini, O., Weiss, J., Duval, P., and Montagnat, M.: Concerning continuum damage mechanics applied to crevassing and icebergs calving, Comment on: Duddu and Waisman (2012a, b), *J. Glaciol.*, 59, 797–798, 2013a. 1119

Gagliardini, O., Zwinger, T., Gillet-Chaulet, F., Durand, G., Favier, L., de Fleurian, B., Greve, R., Malinen, M., Martín, C., Råback, P., Ruokolainen, J., Sacchetti, M., Schäfer, M., Seddik, H.,

Combining damage and fracture mechanics to model calving

J. Krug et al.

Title Page

Abstract

Introduction

Conclusions

References

Tables

Figures

◀

▶

◀

▶

Back

Close

Full Screen / Esc

Printer-friendly Version

Interactive Discussion

- and Thies, J.: Capabilities and performance of Elmer/Ice, a new-generation ice sheet model, *Geosci. Model Dev.*, 6, 1299–1318, doi:10.5194/gmd-6-1299-2013, 2013b. 1125
- Gillet-Chaulet, F., Gagliardini, O., Seddik, H., Nodet, M., Durand, G., Ritz, C., Zwinger, T., Greve, R., and Vaughan, D. G.: Greenland ice sheet contribution to sea-level rise from a new-generation ice-sheet model, *The Cryosphere*, 6, 1561–1576, doi:10.5194/tc-6-1561-2012, 2012. 1127
- Glinka, G.: Development of weight functions and computer integration procedures for calculating stress intensity factors around cracks subjected to complex stress fields, *Progress Report No. 1, Stress and Fatigue-Fracture Design*, Petersburg, 1996. 1123, 1134
- Hayhurst, D.: Creep rupture under multi-axial states of stress, *J. Mech. Phys. Solids*, 20, 381–382, 1972. 1119
- Howat, I. M., Joughin, I., and Scambos, T. A.: Rapid changes in ice discharge from Greenland outlet glaciers, *Science*, 315, 1559–1561, 2007. 1125, 1127
- Jay-Allemand, M., Gillet-Chaulet, F., Gagliardini, O., and Nodet, M.: Investigating changes in basal conditions of Variegated Glacier prior to and during its 1982–1983 surge, *The Cryosphere*, 5, 659–672, doi:10.5194/tc-5-659-2011, 2011. 1116
- Joughin, I., Das, S. B., King, M. A., Smith, B. E., Howat, I. M., and Moon, T.: Seasonal speedup along the western flank of the Greenland Ice Sheet, *Science*, 320, 781–783, 2008a. 1113
- Joughin, I., Howat, I., Alley, R. B., Ekstrom, G., Fahnestock, M., Moon, T., Nettles, M., Truffer, M., and Tsai, V. C.: Ice-front variation and tidewater behavior on Helheim and Kangerdlugssuaq Glaciers, Greenland, *J. Geophys. Res.-Earth*, 113, F01004, doi:10.1029/2007JF000837, 2008. 1125, 1129, 1132
- Jouvet, G., Picasso, M., Rappaz, J., Huss, M., and Funk, M.: Modelling and Numerical Simulation of the Dynamics of Glaciers Including Local Damage Effects, *Math. Model. Nat. Phenomena*, 6, 263–280, 2011. 1117
- Kachanov, L.: Time of the rupture process under creep conditions, *Isv. Akad. Nauk. SS R. Otd Tekh. Nauk.*, 8, 26–31, 1958. 1113, 1117
- Labbens, R., Pellissier-Tanon, A., and Heliot, J.: Application de la théorie linéaire de la mécanique de la rupture aux structures métalliques épaisses-Méthodes pratiques de calcul des facteurs d'intensité de contrainte, *Rev. Phys. Appl.*, 9, 587–598, 1974. 1122, 1123
- Lemaitre, J., Chaboche, J., and Germain, P.: *Mécanique des Matériaux Solides*, vol. 7, Dunod, Paris, 1988. 1117, 1118

Combining damage and fracture mechanics to model calving

J. Krug et al.

Title Page

Abstract

Introduction

Conclusions

References

Tables

Figures

⏪

⏩

◀

▶

Back

Close

Full Screen / Esc

Printer-friendly Version

Interactive Discussion

- Luckman, A., Murray, T., De Lange, R., and Hanna, E.: Rapid and synchronous ice-dynamic changes in East Greenland, *Geophys. Res. Lett.*, 33, L03503, doi:10.1029/2005GL025428, 2006. 1125
- Ma, Y., Gagliardini, O., Ritz, C., Gillet-Chaulet, F., Durand, G., and Montagnat, M.: Enhancement factors for grounded ice and ice shelves inferred from an anisotropic ice-flow model, *J. Glaciol.*, 56, 805–812, 2010. 1115
- Mottram, R. H. and Benn, D. I.: Testing crevasse-depth models: a field study at Breioamerkurjokull, Iceland, *J. Glaciol.*, 55, 746–752, 2009. 1113, 1121, 1131
- Murakami, S. and Ohno, N.: A continuum theory of creep and creep damage, in: *Creep in Structures*, Springer, 422–444, Toyohashi, 440, Japan 1981. 1118
- Nath, P. and Vaughan, D.: Subsurface crevasse formation in glaciers and ice sheets, *J. Geophys. Res.-Sol. Ea.*, 108, ECV–7, doi:10.1029/2001JB000453, 2003. 1121
- Nick, F. M., Vieli, A., Howat, I. M., and Joughin, I.: Large-scale changes in Greenland outlet glacier dynamics triggered at the terminus, *Nat. Geosci.*, 2, 110–114, 2009. 1125, 1126, 1127
- Nick, F. M., van der Veen, C. J., Vieli, A., and Benn, D. I.: A physically based calving model applied to marine outlet glaciers and implications for the glacier dynamics, *J. Glaciol.*, 56, 781–794, 2010. 1113
- Nick, F. M., Vieli, A., Andersen, M. L., Joughin, I., Payne, A., Edwards, T. L., Pattyn, F., and van de Wal, R. S.: Future sea-level rise from Greenland's main outlet glaciers in a warming climate, *Nature*, 497, 235–238, 2013. 1113
- Nye, J.: The distribution of stress and velocity in glaciers and ice-sheets, *P. R. Soc. Lond. A-Mat.*, 239, 113–133, 1957. 1113
- Otero, J., Navarro, F. J., Martin, C., Cuadrado, M. L., and Corcuera, M. I.: A three-dimensional calving model: numerical experiments on Johnsons Glacier, Livingston Island, Antarctica, *J. Glaciol.*, 56, 200–214, 2010. 1113
- Pralong, A. and Funk, M.: Dynamic damage model of crevasse opening and application to glacier calving, *J. Geophys. Res.*, 110, 12 pp., doi:10.1029/2004JB003104, 2005. 1113, 1117, 1118, 1119, 1120, 1128, 1131
- Pralong, A., Funk, M., and Lüthi, M. P.: A description of crevasse formation using continuum damage mechanics, *Ann. Glaciol.*, 37, 77–82, 2003. 1113, 1117, 1120
- Ravi-Chandar, K. and Knauss, W.: An experimental investigation into dynamic fracture: I. Crack initiation and arrest, *Int. J. Fracture*, 25, 247–262, 1984. 1124

**Combining damage
and fracture
mechanics to model
calving**

J. Krug et al.

Title Page

Abstract

Introduction

Conclusions

References

Tables

Figures

◀

▶

◀

▶

Back

Close

Full Screen / Esc

Printer-friendly Version

Interactive Discussion

- Rignot, E. and Kanagaratnam, P.: Changes in the velocity structure of the Greenland Ice Sheet, *Science*, 311, 986–990, 2006. 1112
- Rignot, E., Koppes, M., and Velicogna, I.: Rapid submarine melting of the calving faces of West Greenland glaciers, *Nat. Geosci.*, 3, 187–191, 2010. 1112, 1127
- 5 Rist, M. A., Sammonds, P. R., Murrell, S. A. F., Meredith, P. G., Oerter, H., and Doake, C. S. M.: Experimental fracture and mechanical properties of Antarctic ice preliminary results, *Ann. Glaciol.*, 23, 284–292, 1996. 1123
- Rist, M. A., Sammonds, P. R., Murrell, S. A. F., Meredith, P. G., Doake, C. S. M., Oerter, H., and Matsuki, K.: Experimental and theoretical fracture mechanics applied to Antarctic ice fracture and surface crevassing, *J. Geophys. Res.*, 104, 2973–2987, 1999. 1118, 1121
- 10 Scambos, T. A., Bohlander, J., Shuman, C., and Skvarca, P.: Glacier acceleration and thinning after ice shelf collapse in the Larsen B embayment, *Antarctica, Geophys. Res. Lett.*, 31, L18402, doi:10.1029/2004GL020670, 2004. 1112
- Schulson, E. M. and Duval, P.: *Creep and fracture of ice*, Cambridge University Press, Cambridge, 2009. 1123
- 15 Shepherd, A., Ivins, E. R., Geruo, A., Barletta, V. R., Bentley, M. J., Bettadpur, S., Briggs, K. H., Bromwich, D. H., Forsberg, R., Galin, N., Horwath, M., Jacobs, S., Joughin, I., King, M. A., Lenaerts, J. T. M., Li, J., Ligtenberg, S. R. M., Luckman, A., Luthcke, S. B., McMillan, M., Meister, R., Milne, G., Mougintot, J., Muir, A., Nicolas, J. P., Paden, J., Payne, A. J., Pritchard, H., Rignot, E., Rott, H., Sandberg Sørensen, L., Scambos, T. A., Scheuchl, B., Schrama, E. J. O., Smith, B., Sundal, A. V., van Angelen, J. H., van de Berg, W. J., van den Broeke, Michiel R. Vaughan, D. G., Velicogna, I., Wahr, J., Whitehouse, P. L., Wingham, D. J., Yi, D., Young, D., and Zwally, H. J.: A reconciled estimate of ice-sheet mass balance, *Science*, 338, 1183–1189, 2012. 1112
- 20 Smith, R. A.: The application of fracture mechanics to the problem of crevasse penetration, *J. Glaciol.*, 17, 223–228, 1976. 1121
- van der Veen, C.: Fracture mechanics approach to penetration of surface crevasses on glaciers, *Cold Reg. Sci. Technol.*, 27, 31–47, 1997. 1113, 1121, 1123, 1124
- van der Veen, C.: Fracture mechanics approach to penetration of bottom crevasses on glaciers, *Cold Reg. Sci. Technol.*, 27, 213–223, 1998. 1113, 1121, 1122, 1123
- 30 Vaughan, D. G.: Relating the occurrence of crevasses to surface strain rates, *J. Glaciol.*, 39, 255–266, 1993. 1119

Weiss, J.: Subcritical crack propagation as a mechanism of crevasse formation and iceberg calving, *J. Glaciol.*, 50, 109–115, 2004. 1121

Weiss, J. and Schulson, E. M.: Coulombic faulting from the grain scale to the geophysical scale: lessons from ice, *J. Phys. D*, 42, 214017, doi:10.1088/0022-3727/42/21/214017, 2009. 1119

5 Xiao, J. and Jordaan, I.: Application of damage mechanics to ice failure in compression, *Cold Reg. Sci. Technol.*, 24, 305–322, 1996. 1117

TC D

8, 1111–1150, 2014

Combining damage and fracture mechanics to model calving

J. Krug et al.

Title Page

Abstract

Introduction

Conclusions

References

Tables

Figures



Back

Close

Full Screen / Esc

Printer-friendly Version

Interactive Discussion



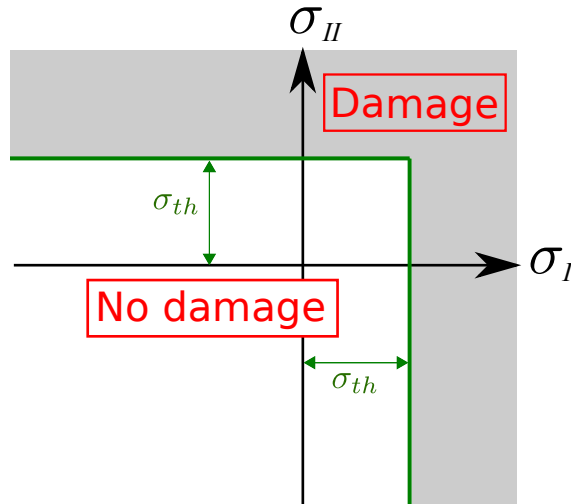


Fig. 1. Damage envelope in the space of principal stresses. σ_I and σ_{II} respectively represent the first principal stress and the second principal stress, and σ_{th} is the stress threshold. The shaded area corresponds to the stress conditions under which damage occurs.

Combining damage and fracture mechanics to model calving

J. Krug et al.

Title Page	
Abstract	Introduction
Conclusions	References
Tables	Figures
◀	▶
◀	▶
Back	Close
Full Screen / Esc	
Printer-friendly Version	
Interactive Discussion	



Combining damage and fracture mechanics to model calving

J. Krug et al.

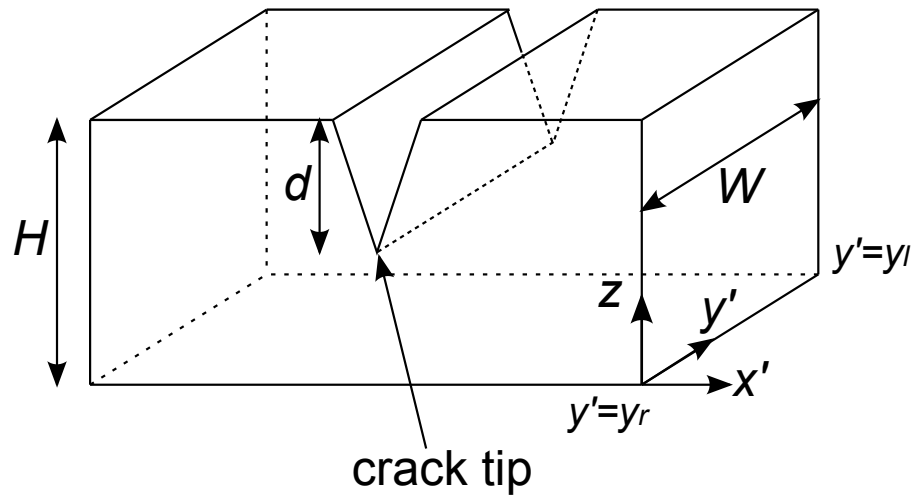


Fig. 2. Crevasse shape. H refers to the ice thickness and d is the crevasse depth.

Title Page

Abstract

Introduction

Conclusions

References

Tables

Figures

◀

▶

◀

▶

Back

Close

Full Screen / Esc

Printer-friendly Version

Interactive Discussion

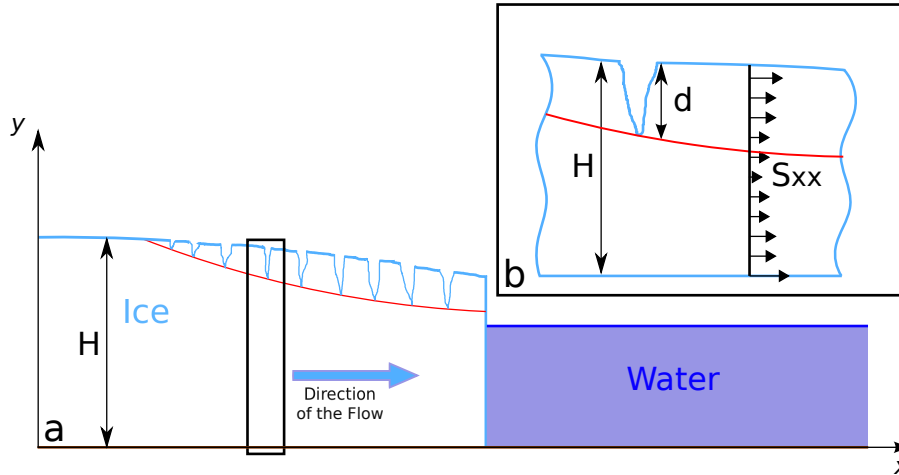


Fig. 3. (a) Shape of a grounded glacier and (b) zoom on the black rectangle. The red curve illustrates the contour of critical damage $D = D_c$ for which we compute the along-flow component of the deviatoric stress tensor S_{xx} multiplied by the weight function and integrated over the crevasse depth d .

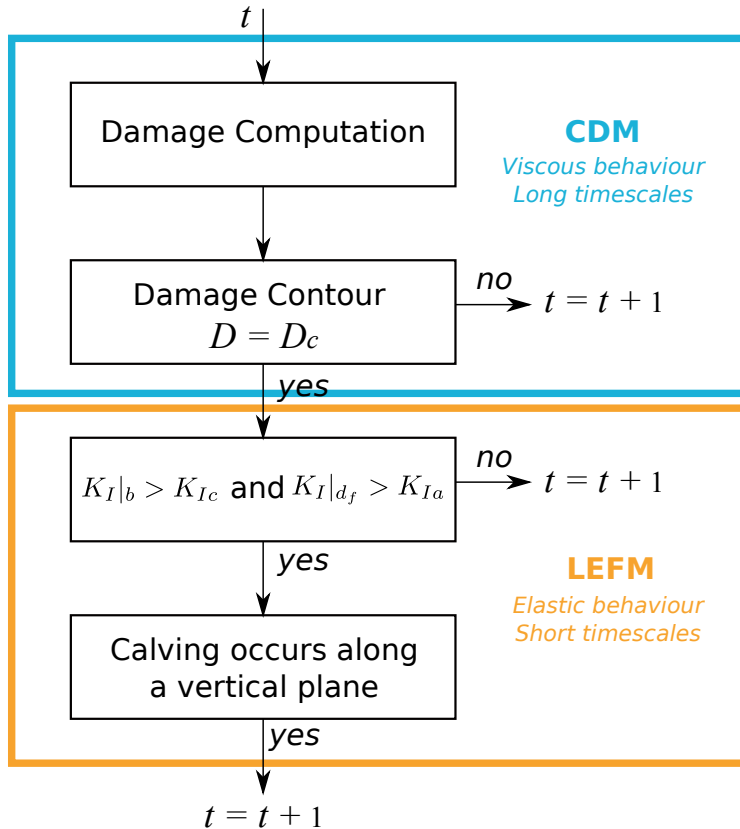


Fig. 4. Algorithm of the calving model where t refers to the time step. Blue shape indicates the area of CDM application, where ice undergoes a viscous behaviour and orange shape corresponds to the LEFM domain of application, where ice has an elastic behaviour, representing fracture propagation and calving event.

Combining damage and fracture mechanics to model calving

J. Krug et al.

Title Page	
Abstract	Introduction
Conclusions	References
Tables	Figures
◀	▶
◀	▶
Back	Close
Full Screen / Esc	
Printer-friendly Version	
Interactive Discussion	



Combining damage and fracture mechanics to model calving

J. Krug et al.

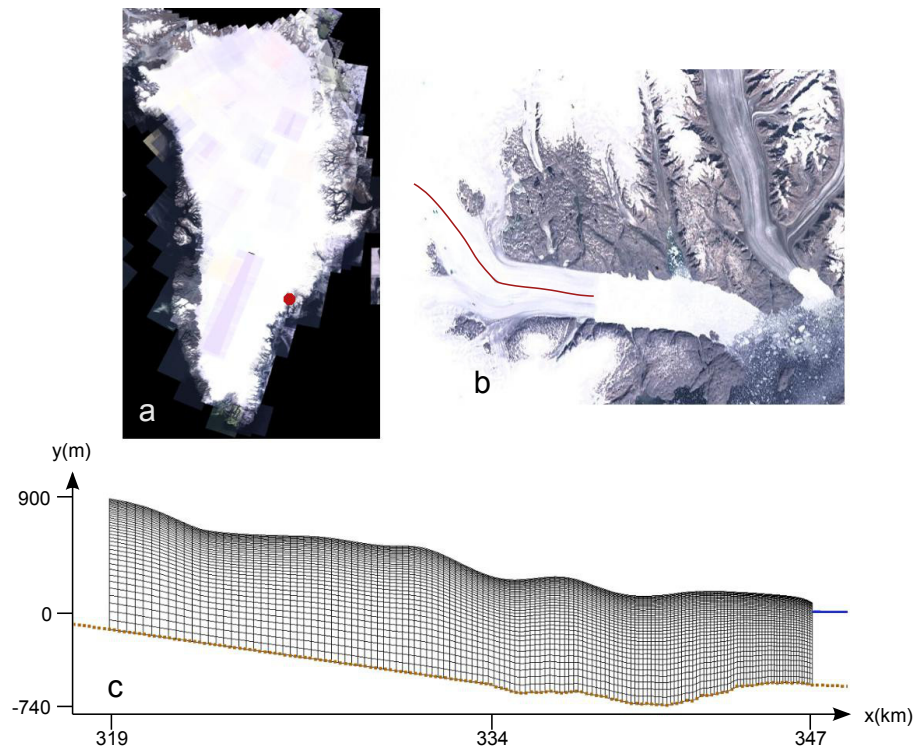


Fig. 5. Glacier location and geometry. **(a)** Location on the Greenland Ice Sheet (red point). **(b)** Zoom on the Helheim terminus and the considered flowline (red curve). **(c)** Mesh extracted from this flowline. The starting position correspond to the front position at 347 km. The blue line represents the sea level.

Combining damage and fracture mechanics to model calving

J. Krug et al.

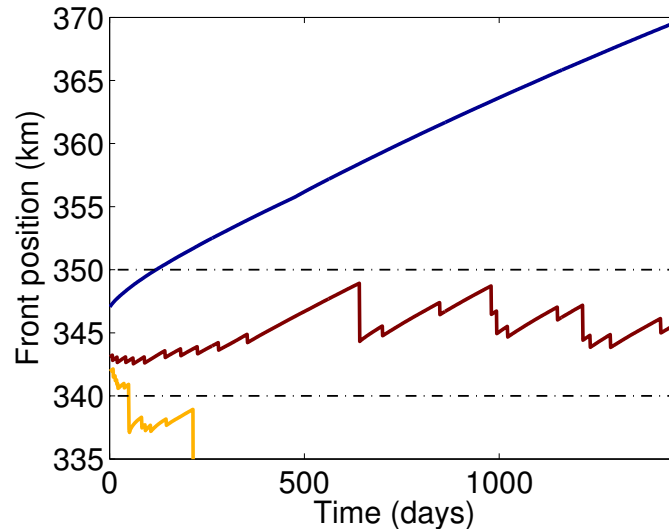


Fig. 6. Position of the calving front as a function of time. Each color correspond to a set of parameter $\bar{\sigma}_{th}$, B , and D_c . The blue color represents an advance with almost no calving ($\bar{\sigma}_{th} = 0.180$ MPa, $B = 1.878$ MPa $^{-1}$, and $D_c = 0.460$); the yellow one corresponds to a severe retreat ($\bar{\sigma}_{th} = 0.112$ MPa, $B = 2.892$ MPa $^{-1}$, and $D_c = 0.528$); the red one presents a behaviour consistent against observations ($\bar{\sigma}_{th} = 0.072$ MPa, $B = 1.870$ MPa $^{-1}$, and $D_c = 0.529$). The yellow curve stopped after 200 days because the glacier retreated too far inland.

[Title Page](#)
[Abstract](#)
[Introduction](#)
[Conclusions](#)
[References](#)
[Tables](#)
[Figures](#)
[⏪](#)
[⏩](#)
[◀](#)
[▶](#)
[Back](#)
[Close](#)
[Full Screen / Esc](#)
[Printer-friendly Version](#)
[Interactive Discussion](#)

Combining damage and fracture mechanics to model calving

J. Krug et al.

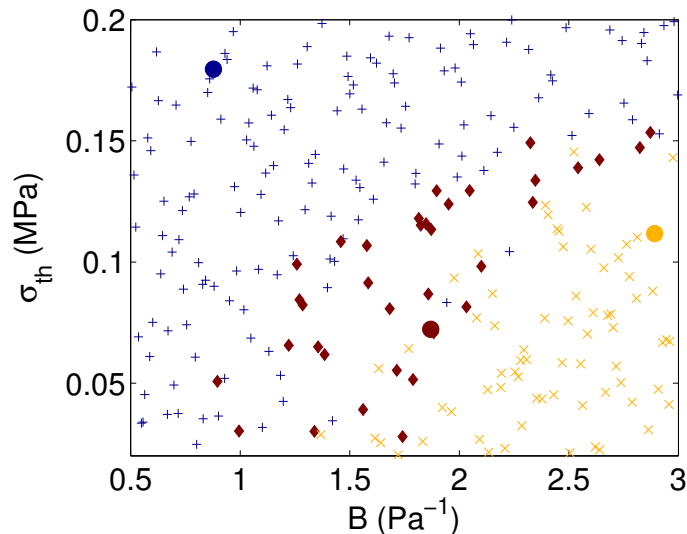


Fig. 7. Sampling in the space of damage parameters B , $\overline{\sigma_{th}}$. Blue plus signs, and yellow crosses respectively represent simulations for which the front exceeded 350 km and simulation for which the front retreated below 340 km. Red diamonds represent the successful simulations. Blue, red and yellow circles corresponds to the same colored curves in Fig. 6. Red circle corresponds to the simulation illustrated on Fig. 8.

Title Page

Abstract

Introduction

Conclusions

References

Tables

Figures

◀

▶

◀

▶

Back

Close

Full Screen / Esc

Printer-friendly Version

Interactive Discussion

Combining damage and fracture mechanics to model calving

J. Krug et al.

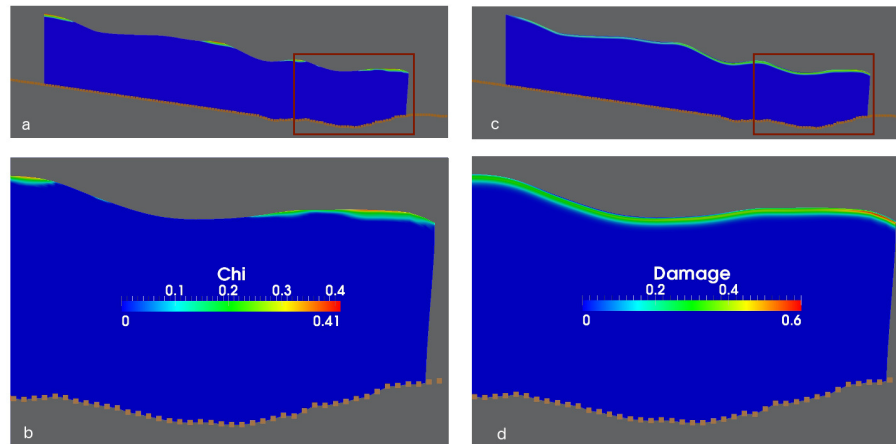


Fig. 8. State of Helheim glacier after 365 days of simulation for the set of parameter ($\overline{\sigma_{th}} = 0.072 \text{ MPa}$, $B = 1.870 \text{ MPa}^{-1}$, and $D_c = 0.529$) corresponding to the red circle on Fig. 7. **(a)** Damaging areas of Helheim glacier and **(b)** zoom on the red rectangle; **(c)** Damage field and zoom on the red rectangle **(d)**.

[Title Page](#)
[Abstract](#)
[Introduction](#)
[Conclusions](#)
[References](#)
[Tables](#)
[Figures](#)
[⏪](#)
[⏩](#)
[◀](#)
[▶](#)
[Back](#)
[Close](#)
[Full Screen / Esc](#)
[Printer-friendly Version](#)
[Interactive Discussion](#)

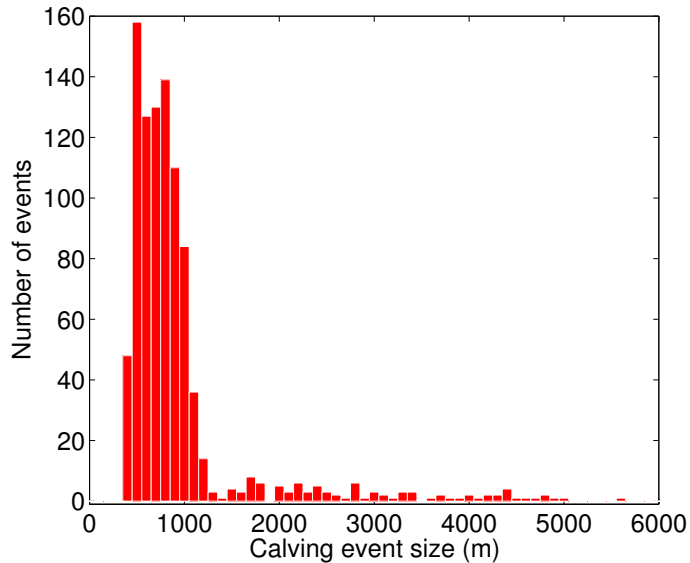


Fig. 9. Distribution of calving event sizes for the 36 realistic simulations.

Combining damage and fracture mechanics to model calving

J. Krug et al.

Title Page

Abstract Introduction

Conclusions References

Tables Figures

⏪ ⏩

◀ ▶

Back Close

Full Screen / Esc

Printer-friendly Version

Interactive Discussion

